Inorg. Chem. **2008**, *47*, 10906−10910

Cyclic Boron Clusters Enclosing Planar Hypercoordinate Cobalt, Iron, and Nickel

Keigo Ito,[†] Zhifeng Pu,[‡] Qian-Shu Li,[*,‡,§] and Paul von Ragué Schleyer[*,†]

Department of Chemistry, Center for Computational Chemistry, University of Georgia, Athens, Georgia 30602, U.S.A., School of Chemical Engineering and the Environment, Beijing Institute of Technology, Beijing 100081, China, and Center for Computational Quantum Chemistry, South China Normal University, Guangzhou 510631, China

Received May 30, 2008

Planar cyclic boron clusters with cobalt, iron, and nickel atoms at their centers—singlet D_{8h} CoB_8^-, D_{9h} FeB_9^-, CoB_9, and NiB_9^+—are computed to be stable minima at the BP86/TZVPP DFT level. Stochastic searches of the singlet and triplet potential energy surfaces show the planar hypercoordinate D_{8h} CoB_8^- (**1**) and D_{9h} FeB_9^- (**2**) singlet isomers to be the global minima. Their double aromatic character with 6 π and 10 radial electrons is documented by detailed $NICS_{zz}$ grid and CMO-$NICS_{zz}$ analyses at PW91/TZVPP. These results encourage gas phase investigations of these two exotic anions. Although isoelectronic with D_{9h} FeB_9^- (**2**), CoB_9 and NiB_9^+ prefer nonplanar structures, triplet **3-aT** for the former and singlet **4-a** for the latter.

Introduction

Molecules exhibiting planar hypercoordination captivate chemists because of their extreme violations of classical bonding principles.[1−7] Although the tetrahedral tetracoordination of carbon was proposed by van't Hoff[8] and Le Bel[9] in 1874, Monkhorst (1968) was the first to compute methane in its very high energy D_{4h} planar geometry.[10] Hoffmann, Alder, and Wilcox suggested strategies to stabilize planar tetracoordinate carbon (ptC) transition states in 1970,[11] but the first planar ptC *minimum* was computed by Schleyer, Pople, and co-workers in 1976.[12] Since then, numerous ptCs have been described, both experimentally and computationally.[1−6] A notable example is the 1999 Wang−Boldyrev−Simons verification[13] of the 1991 Schleyer−Boldyrev prediction of ptCs having only five atoms.[14] Even higher planar hypercoordination of carbon, for example, D_{6h} CB_6^{2-} [15] and many other of its hexacoordinate relatives are local minima.[16,17] Numerous planar pentacoordinate carbon molecules, as well as the planar heptacoordinate carbon D_{7h} CB_7^- and the octacoordinate silicon D_{8h} SiB_8, were computed by Wang and Schleyer in 2001.[18] The D_{5h} pentacoordinate carbon CAl_5^+ cation has just been identified as being the global minimum.[19] The Hückel aromaticity of these planar species contributes to their stability.

Although such unusual arrangements of carbon are startling, planar hypercoordination of other elements are just as

* To whom correspondence should be addressed. E-mail: qsli@bit.edu.cn (Q.S.L.), schleyer@chem.uga.edu (P.v.R.S.).
† University of Georgia.
‡ Beijing Institute of Technology.
§ South China Normal University.

(1) Sorger, K.; Schleyer, P. v. R. *J. Mol. Struct. (THEOCHEM)* **1995**, *338*, 317–346.
(2) Röttger, D.; Erker, G. *Angew. Chem., Int. Ed. Engl.* **1997**, *36*, 812–827.
(3) Radom, L.; Rasmussen, D. R. *Pure Appl. Chem.* **1998**, *70*, 1977–1984.
(4) Siebert, W.; Gunale, A. *Chem. Soc. Rev.* **1999**, *28*, 367–371.
(5) Keese, R. *Chem. Rev.* **2006**, *106*, 4787–4808.
(6) Merino, G.; Méndes-Rojas, M. A.; Vela, A.; Heine, T. *J. Comput. Chem.* **2007**, *28*, 362–372.
(7) Merino, G.; Méndes-Rojas, M. A.; Beltrán, H. I.; Corminboeuf, C.; Heine, T.; Vela, A. *J. Am. Chem. Soc.* **2004**, *126*, 16160–16169.
(8) van't Hoff, J. H. *Arch. Neerl. Sci. Exactes Nat.* **1874**, *9*, 445–454.
(9) Le Bel, J. A. *Bull. Soc. Chim. Fr.* **1874**, *22*, 337–347.
(10) Monkhorst, H. *Chem. Commun.* **1968**, *18*, 1111–1112.
(11) Hoffmann, R.; Alder, R. W.; Wilcox, C. F. *J. Am. Chem. Soc.* **1970**, *92*, 4992–4993.
(12) Collins, J. B.; Dill, J. D.; Jemmis, E. D.; Apeloig, Y.; Schleyer, P. v. R.; Seeger, R.; Pople, J. A. *J. Am. Chem. Soc.* **1976**, *98*, 5419–5427.
(13) Li, X.; Wang, L.-S.; Boldyrev, A. I.; Simons, J. *J. Am. Chem. Soc.* **1999**, *121*, 6033–6038.
(14) Schleyer, P. v. R.; Boldyrev, A. I. *J. Chem. Soc., Chem. Commun.* **1991**, 1536–1538.
(15) Exner, K.; Schleyer, P. v. R. *Science* **2000**, *290*, 1937–1940.
(16) Minyaev, R. M.; Gribanova, T. N. *Russ. Chem. Bull.* **2000**, *49*, 783–793.
(17) Ito, K.; Chen, Z.; Corminboeuf, C.; Wannere, C.; Zhang, X.-H.; Li, Q.-S.; Schleyer, P. v. R. *J. Am. Chem. Soc.* **2007**, *129*, 1510–1512.
(18) Wang, Z.-X.; Schleyer, P. v. R. *Science* **2001**, *292*, 2465–2469.
(19) Pei, Y.; An, W.; Ito, K.; Schleyer, P. v. R.; Zeng, X. C. *J. Am. Chem. Soc.* **2008**, *130*, 10394–10400.

10.1021/ic800993b CCC: $40.75
Published on Web 10/29/2008

interesting. Bonačić−Koutecký et al. computed the first theoretical molecules containing a planar hexacoordinate boron in 1991.[20] In addition, there are examples of hypercoordinate nitrogen, oxygen,[14] phosphorus, germanium, tin, etc.[20–27] Notably, anions with planar hypercoordinate borons, B_8^- and B_9^-, were characterized by photoelectron spectroscopy in the gas phase by Boldyrev, Wang, and co-workers.[28] Their computational study indicated that these species are doubly aromatic,[29] due to the presence of six π and six radial electrons.

The concept of planar hypercoordination is not restricted to main group elements. Pseudoplanar hypercoordinate transition metal derivatives include Ni(TBC),[30] $[Ni(Pt-Bu)_6]$[31] and $[In(Mn(CO)_4)_5]$.[32] Steric repulsion of the substituent groups in those molecules helps to achieve planarity. Frenking et al.[33] computed planar hypercoordinate transition metal (phTM) minima, singlet D_{5h} $FeBi_5^-$ and $FeSb_5^-$, in 2003. However, they found that the triplet C_s isomers were more stable than the D_{5h} singlets. Other phTMs, such as MAu_6^- (M = Ti, V, Cr),[34] Au_5Zn^+,[35] and Cu_7Sc,[36] also have been investigated, as have transition metal (TM)-doped planar and nonplanar boron clusters.[37−42]

We now report theoretical predictions of planar B_8 and B_9 boron ring encapsulation of octa- and nonacoordinate cobalt, iron, and nickel, which parallel Qiong's recent and somewhat similar independent study.[42] Boron participates especially well in multicenter bonding due to its electron deficient character.[43] Our phTM designs were based on the Schleyer−Boldyrev geometrical and electronic match principles.[14] The size of the boron ligand ring must match the optimum lengths of the B−TM multicenter bonds between the central TM and the peripheral ligand atoms. The charge of the species is chosen on the basis of electron occupancy considerations to maximize the favorable TM−B bonding interactions.

Computational Methods

Geometry optimization and harmonic vibrational frequency computations at the BP86[44−46] DFT level with the TZVPP[47] basis set employed the Gaussian 03 program.[48] No wave function instabilities were found. Natural population analysis (NPA)[49] charge computations and Wiberg bond indices (WBI)[50] were computed at the same level using NBO 5.G.[51] Grids of nucleus-independent chemical shifts (NICS)[52,53] and their *zz* NICS shielding tensor components ($NICS_{zz}$)[54] were performed with the PW91 functional[55] and the TZVPP[47] basis set using the gauge including atomic orbital (GIAO)[56] method. Although NICS values are insensitive to the density functionals, it has been found that chemical shift computations are more accurate at PW91, so that this level was employed here.[57] The $NICS_{zz}$ shielding tensors also were dissected into the contributions of individual canonical molecular orbitals (CMO-$NICS_{zz}$).[58,59] Potential energy surface scans of phTM species were performed using Saunders' "Kick" stochastic search method.[60−62] A total of 3000 structures (singlet, triplet, or quintet) were randomly generated for each phTM species in a constrained box, which was varied from 2.5 to 4.0 Å. The initial Kick geometries were optimized first at the HF/STO-3G level of theory. All unique structures obtained from this initial Kick search were then reoptimized at the

(20) Bonačić-Koutecký, V.; Fantucci, P.; Koutecký, J. *Chem. Rev.* **1991**, *91*, 1035–1108.
(21) Driess, M.; Aust, J.; Merz, K.; van Wüllen, C. *Angew. Chem., Int. Ed.* **1999**, *38*, 3677–3680.
(22) Gribanova, T. N.; Minyaev, R. M.; Minkin, V. I. *Mendeleev Commun.* **2001**, 169–170.
(23) Li, S.-D.; Miao, C.-Q.; Ren, G.-M. *Eur. J. Inorg. Chem.* **2004**, 2232–2234.
(24) Li, S.-D.; Ren, G.-M.; Miao, C.-Q.; Jin, Z.-H. *Angew. Chem., Int. Ed.* **2004**, *43*, 1371–1373.
(25) Li, S.-D.; Ren, G.-M.; Miao, C.-Q. *Inorg. Chem.* **2004**, *43*, 6331–6333.
(26) Li, S.-D.; Miao, C.-Q. *J. Phys. Chem. A* **2005**, *109*, 7594–7597.
(27) Islas, R.; Heine, T.; Ito, K.; Schleyer, P. v. R.; Merino, G. *J. Am. Chem. Soc.* **2007**, *129*, 14767–14774.
(28) Zhai, H.-J.; Alexandrova, A. N.; Birch, K. A.; Boldyrev, A. I.; Wang, L.-S. *Angew. Chem., Int. Ed. Engl.* **2003**, *42*, 6004–6008.
(29) Chandrasekhar, J.; Jemmis, E. D.; Schleyer, P. v. R. *Tetrahedron Lett.* **1979**, *39*, 3707–3710.
(30) Ferrara, J. D.; Tanaka, A. A.; Fierro, C.; Tessier-Youngs, C. A.; Youngs, W. J. *Organometallics* **1989**, *8*, 2089–2098.
(31) Ahlrichs, R.; Fenske, D.; Oesen, H.; Schneider, U. *Angew. Chem., Int. Ed. Engl.* **1992**, *31*, 323–326.
(32) Schollenberger, M.; Nuber, B.; Ziegler, M. *Angew. Chem., Int. Ed. Engl.* **1992**, *31*, 350–351.
(33) Lein, M.; Frunzke, J.; Frenking, G. *Angew. Chem., Int. Ed.* **2003**, *42*, 1303–1306.
(34) Li, X.; Kiran, B.; Cui, L.-F.; Wang, L.-S. *Phys. Rev. Lett.* **2005**, *95,* 253401−1−253401−4.
(35) Tanaka, H.; Neukermans, S.; Janssens, E.; Silverans, R.; Lievens, P. *J. Am. Chem. Soc.* **2003**, *125*, 2862–2863.
(36) Höltzl, T.; Janssens, E.; Veldeman, N.; Veszprémi, T.; Lievens, P.; Nguyen, M. T. *Chem. Phys. Chem.* **2008**, *9*, 833–838.
(37) Garnovsky, A. D.; Bren, V. A. *ARKIVOC* **2005**, *2005*, 1–10.
(38) Li, S.-D.; Miao, C.-Q.; Ren, G.-M.; Guo, J.-C. *Eur. J. Inorg. Chem.* **2006**, 2567–2571.
(39) Liu, X. L.; Zhao, G.-F.; Guo, L.-J.; Jing, Q.; Luo, Y.-H. *Phys. Rev. A* **2007**, *75*, 063201−1−063201−6.
(40) Yang, Z.; Xiong, S.-J. *J. Chem. Phys.* **2008**, *128*−1−8.
(41) Yao, J.-G.; Wang, X.-W.; Wang, Y.-X. *Chem. Phys.* **2008**, *351*, 1–6.
(42) Qiong, L. *Sci. China, Ser. B: Chem.* **2008**, *51*, 1–7.
(43) Averkiev, B. B.; Zubarev, D. Y.; Wang, L.-M.; Huang, W.; Wang, L.-S.; Boldyrev, A. I. *J. Am. Chem. Soc.* **2008**, *130*, 9248–9250.
(44) Becke, A. D. *Phys. Rev. A* **1988**, *38*, 3098–3100.
(45) Perdrew, J. P. *Phys. Rev. B* **1986**, *33*, 8822–8824.
(46) Jensen et al. concluded that, for molecules containing first row transition metal atoms, the BP86 functional performed slightly better than hybrid functionals, such as B3LYP. For more details, see: Jensen, K. P.; Roos, B. O.; Ryde, U. *J. Chem. Phys.* **2007**, *126*, 014103−1−014103−14.
(47) Weigend, F.; Haeser, M.; Patzelt, H.; Ahlrichs, R. *Chem. Phys. Lett.* **1998**, *294*, 143–152.
(48) Frisch, M. J. *Gaussian 03, Revision C.02*; Gaussian, Inc.: Wallingford, CT, 2004.
(49) Reed, A. E.; Weinstock, R. B.; Weinhold, F. *J. Chem. Phys.* **1985**, *83*, 735–746.
(50) Wiberg, K. B. *Tetrahedron* **1968**, *24*, 1083–1096.
(51) Glendening, E. D.; Badenhoop, J. K.; Reed, A. E.; Carpenter, J. E.; Bohmann, J. A.; Morales, C. M.; Weinhold, F. *NBO, 5.G*; University of Wisconsin: Madison, WI, 2001.
(52) Schleyer, P. v. R.; Maerker, C.; Dransfeld, A.; Jiao, H.; Hommes, N. J. R. v. E. *J. Am. Chem. Soc.* **1996**, *118*, 6317–6318.
(53) Schleyer, P. v. R.; Jiao, H.; Hommes, N. J. R. v. E.; Malkin, V. G.; Malkina, O. L. *J. Am. Chem. Soc.* **1997**, *119*, 12669–12670.
(54) Steiner, E.; Fowler, P. W.; Jenneskens, L. W. *Angew. Chem., Int. Ed.* **2001**, *40*, 362–366.
(55) Perdew, J. P.; Chevary, J. A.; Vosko, S. H.; Kackson, K. A.; Pederson, M. R.; Singh, D. J.; Foiolhais, C. *Phys. Rev. B* **1992**, *46*, 6671–6687.
(56) Ditchfield, R. *Mol. Phys.* **1974**, *27*, 789–807.
(57) Corminboeuf, C.; Heine, T.; Weber, J. *Chem. Phys. Lett.* **2002**, *357*, 1–7.
(58) Corminboeuf, C.; Heine, T.; Weber, J. *Phys. Chem. Chem. Phys.* **2003**, *5*, 246–251.
(59) Fallah-Bagher-Shaidaei, H.; Wannere, C. S.; Corminboeuf, C.; Puchta, R.; Schleyer, P. v. R. *Org. Lett.* **2006**, *8*, 863–866.
(60) Saunders, M. *J. Am. Chem. Soc.* **1987**, *109*, 3150–3152.
(61) Bera, P. P.; Sattelmeyer, K. W.; Saunders, M.; Schaefer, H. F., III.; Schleyer, P. v. R. *J. Phys. Chem. A* **2006**, *110*, 4287–4290.
(62) Loyd, L. D.; Johnston, R. L. *Chem. Phys.* **1998**, *236*, 107–121.

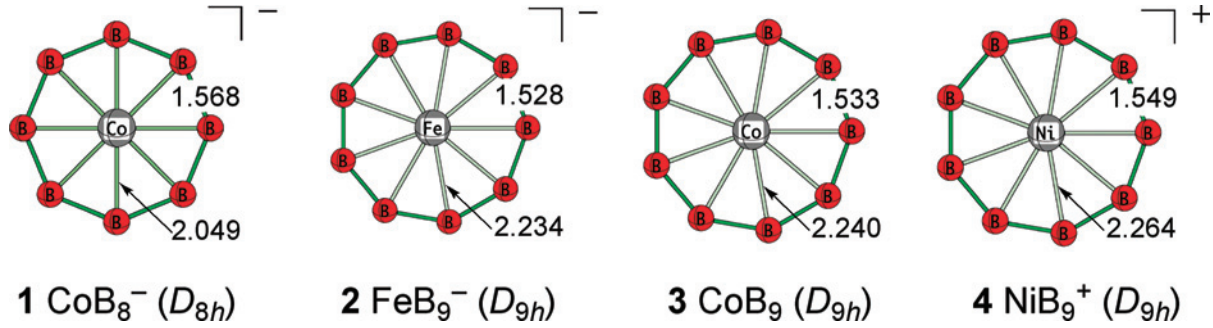

Figure 1. Optimized geometries of the phTM minima at BP86/TZVPP. Bond distances are in angstroms.

BP86/TZVPP level, followed by the harmonic vibrational frequency computations.

Results and Discussion

Geometry and Bonding Analysis. The singlet cyclic boron cluster minima encapsulating the planar hypercoordinate cobalt, iron, or nickel atoms, **1**−**4**, are shown in Figure 1. The Co−B bond distance in **1** (2.049Å, Figure 1) documents the significant bonding, as it is notably shorter than the typical Co−B value (2.16 Å).[63] The transition metal (TM) to boron separations (2.234, 2.240, and 2.264 Å, respectively) in **2**, **3**, and **4** are somewhat longer than the sum of the atomic radii of the TM and boron (2.14, 2.16, and 2.15 Å, respectively),[63] due to the larger cavity size of the nine-membered boron ring. The boron−boron bond distances of **1**−**4** (1.568, 1.528, 1.533, and 1.549 Å, respectively) are significantly shorter than the single boron−boron bond length, 1.622 Å, computed for D_{2d} B_2H_4 at the BP86/TZVPP level. However, the **1**−**4** bond lengths are comparable to the 1.560 Å B═B double bond distance reported by Robinson, et al.[64] The delocalized, multicenter bonding in the phTM species results in short B−B bond distances.

Molecular Orbital (MO) Analysis. As shown by the MO plot (Figure 2), **1** has six π electrons (MOs 26, 27, and 29). The boron ring contribution dominates the a_{2u} π MO (MO 29); there is little cobalt involvement. The energy of the cobalt $3p_z$ atomic orbital (AO) (MO17) is too low to efficiently interact with the boron ring π MO. The a_{2u} MO binds the peripheral boron atoms and helps to retain the planar geometry of **1**. The cobalt involvement is so effective in the degenerate π e_{1g} MO set (MO 26 and 27), formed by the overlap of the $3d_{(xz,yz)}$ cobalt AOs with the boron ring π MOs, that this MO set is lower in energy than the a_{2u} π MO (29). Similar d−π interactions are present in D_{5h} $FeSb_5^+$ and in $FeBi_5^+$.[24] Note that five MOs (25, 30, 31, 33, and 34) have radial bonding character, as they are comprised of in-plane boron $p_{(x,y)}$ AOs pointing toward the center of the ring. The cobalt $3d_{xy}$ and $d_{x^2-y^2}$ AOs effectively overlap with the in-plane radial MOs, producing the bonding MOs (MO 30 and 31). The MOs 33 and 34 are primarily composed by the boron in-plane $p_{(x,y)}$ AOs. Like the a_{2u} π MO, the $3p_{(x,y)}$ involvement is negligible because the $3p_{(x,y)}$ AOs (MO 15 and 16) energies are too low compared to the boron ring radial MO. There is very little bonding between the central cobalt atom and the peripheral borons. In addition, the 4s and $3d_{z^2}$ cobalt AOs mix and interact with the lowest energy radial MO of the B_8 in a bonding and a nonbonding manner. The resulting bonding radial MO 25 joins the central cobalt atom to the peripheral atoms of the boron ring and helps planarize the geometry. MO 32, the formally antibonding Co−B counterpart of MO25, is effectively nonbonding, dominated by the cobalt $3d_{z^2}$ AO. Hence, **1** has radial aromaticity with 10 (rather than 12) radial electrons. The formal electron count of the central cobalt atom in **1** satisfies the 18-electron rule, if MOs 15−17, 25−27, and 30−32 are included. Likewise, the transition metal atoms in **2**−**4** also have a formal 18-electron count, and their MOs are similar to **1** (see Supporting Information Figures 5S−7S). However, the $d_{(xz,yz)}$-π interactions (see Supporting Information Figure 7S, MO 29 and 30) in **4** are diminished such that MOs 29 and 30 are mostly lone pair $d_{(xz,yz)}$. A smaller Ni−B interaction is also evident in the individual Ni−B WBI (WBI_{TM-B}, see the bond index analysis section and Table 1).

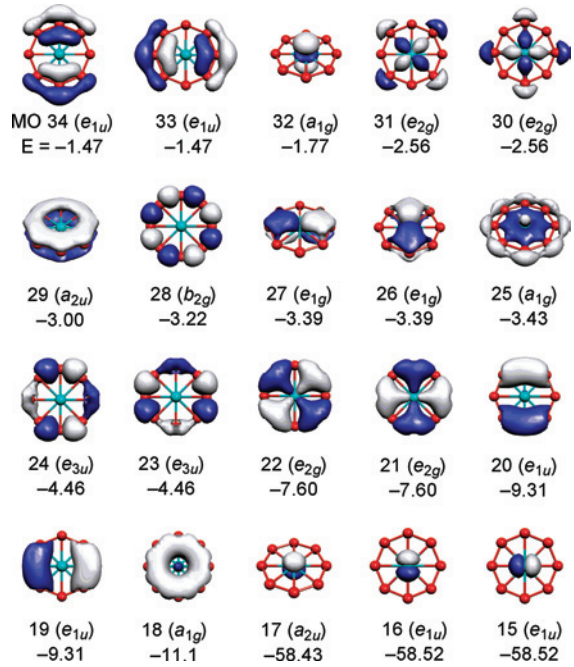

Figure 2. MOs of D_{8h} CoB_8^- (**1**) at the BP86/TZVPP level. MO energies are in eV.

(63) Sutton, L. R. E., *Tables of Interatomic Distances and Configuration in Molecules and Ions*; Supplement 1956−1959; Chemical Society: London, 1965; Vol. *18*.

(64) Wang, Y.; Quillian, B.; Wei, P.; Wannere, C. S.; Xie, Y.; King, R. B.; Schaefer, H. F., III.; Schleyer, P. v. R.; Robinson, G. H. *J. Am. Chem. Soc.* **2007**, *129*, 12412–12413.

Table 1. Summary of the Total Energies ($E_{Tot.}$), the Zero-point Energy Corrections (ZPE), and the TM−B and B−B Bond Distances (r_{TM-B} and r_{B-B})[a]

	$E_{Tot.}$ (a.u.)	ZPE (kcal/mol)	r_{TM-B} (Å)	r_{B-B} (Å)
1	−1581.80024	19.6	2.049	1.568
2	−1487.53869	21.4	2.234	1.528
3	−1606.50693	21.1	2.240	1.533
4	−1731.76914	20.6	2.264	1.549

[a] Computed at the BP86/TZVPP level.

Table 2. Wiberg Bond Indices of the Individual TM−B Bond, TM Total Bond Order, the Individual B−B Bond, the Boron Total Bond Order (WBI_{TM-B}, $WBI_{TMTot.}$, WBI_{B-B} and $WBI_{BTot.}$, Respectively), Natural Population Analysis Charges of the TM and Boron Atoms (NPA_{TM} and NPA_B, respectively), and $NICS(1)_{zz}$ (in ppm)[a]

	WBI_{TM-B}	$WBI_{TMTot.}$	WBI_{B-B}	$WBI_{BTot.}$	NPA_{TM}	NPA_B	$NICS(1)_{zz}$
1	0.39	3.15	1.44	3.61	0.45	−0.18	−84.5
2	0.41	3.71	1.44	3.63	0.54	−0.17	−85.8
3	0.37	3.29	1.40	3.54	0.71	−0.08	−85.4
4	0.28	2.55	1.37	3.44	0.88	0.01	−84.0

[a] WBIs and NPA charges were computed at the BP86/TZVPP level, and $NICS(1)_{zz}$ computations were performed at the PW91/TZVPP level.

Bond Index Analysis. The individual TM−B WBIs (WBI_{TM-B}) of **1**−**4** (0.39, 0.41, 0.37, and 0.28, respectively; see Table 2) reveal appreciable interactions between the TM and peripheral boron atoms. The total WBIs of the central TM atoms ($WBI_{TMTot.}$) range from 2.55 to 3.71 (see Table 2). This implies that each TM−B interaction is weak, but the unusually large number of partial TM−B bonds compensate. The individual boron−boron WBIs (WBI_{B-B}), in the 1.37 to 1.44 range (see Table 2), reflect the enhanced B−B bonding arising from the delocalized π and radial interactions. Moreover, the evenly distributed NPA charges on the peripheral boron atoms (NPA_B, see Table 2) in **1**−**4** further document the delocalized bonding nature of the phTMs.

Magnetic Aromaticity Analysis. The MO plot (Figure 2) suggests that **1** is doubly aromatic[29] due to the presence of 6 π and 10 radial electrons. The $NICS_{zz}$ at a point 1.0 Å above the ring centers ($NICS(1)_{zz}$)[53,54,65] of **1**−**4** range from −84.0 to −85.8 ppm (see Table 2). Such diamagnetic $NICS(1)_{zz}$ values are much larger than those of benzene (−29.0), due to their very strong aromatic character.

More insights into the magnetic aromaticity are given by canonical molecular orbital dissection of $NICS(1)_{zz}$ (CMO-$NICS(1)_{zz}$)[58] of **1**[66] using NBO5.G[51] (see Figure 3). The CMO-$NICS(1)_{zz}$ reveals that the contributions from both the π MOs (−21.7 ppm) and the radial MOs (−51.6) are both strongly diatropic, which depicts a double aromatic character.[29] Note that the total radial MO contribution is more than twice as large as that of the π MO total. Evidently, the radial MOs are even more important than the π MOs in determining the planar geometry preference of **1**.

The magnetic properties of **1** were further elucidated by $NICS_{zz}$ grids (at points spaced 1.0 Å apart) partitioned into contributions from π, radial and d_{z^2} MOs ($NICS_{\pi zz}$, $NICS_{Radzz}$, and $NICS_{dz^2zz}$)[59,65] (Figure 4). Both $NICS_{\pi zz}$ and the $NICS_{Radzz}$ grids reveal cone-shaped regions: diatropic shielding tensors

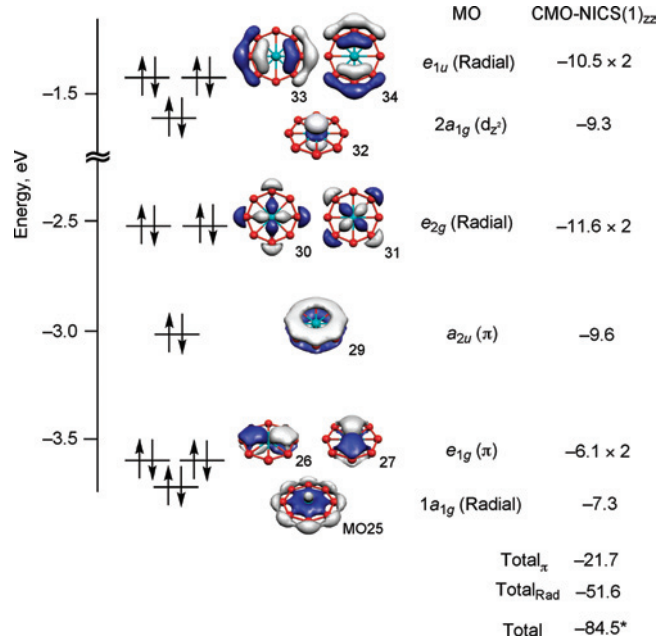

Figure 3. CMO-$NICS(1)_{zz}$ of D_{8h} CoB_8^- (**1**) at PW91/TZVPP level. NICS values are in ppm. *Total $NICS(1)_{zz}$ value includes contributions from core, σ, and d_{z^2} MOs.

(red points) inside and paratropic tensors (green points) outside the ring. These confirm the double aromatic character[29] of D_{8h} CoB_8^-. Such magnetic behavior is consistent with the ring current model[67] and is similar to that of C_5^{2-},[7] CCu_4^{2+},[68] and SiB_8.[27] Despite the nonbonding character of MO 32, its $NICS(1)_{zz}$ tensor contribution from MO 32 is moderately large (−9.3 ppm, see Figures 3 and 4). However, this contribution is only a local effect of the large cobalt $3d_{z^2}$ AO, as its magnitude attenuates quickly further away from the central cobalt atom (Figure 4d).

Chemical Viability.[69] Of the four phTMs discussed here, **1** and **2** are most likely to be observable singlets in the gas phase. Although both are global minima, their HOMO−LUMO gaps (1.27 and 0.97 eV, respectively) and lowest harmonic vibration frequencies ($\nu_{min.}$ = 26.7 and 15.2 cm^{-1}) are rather small (this also is true for **3** and **4**; see Table 3). The $\nu_{min.}$ vectors correspond to out-of-plane pyramidal deformations (a_{2u} mode) for **1** and to out-of-plane ring flopping (degenerate e_{2u} modes) for **2**−**4** (see the Supporting Information, Figures 1S−4S for the results of IRC computations along the lowest real vibrational frequency trajectories). The average atomization energy per atom of **3** (4.84 eV) are comparable to those of D_{8h} SiB_8[27] (4.62 eV at BP86/TZVPP). The vertical detachment energy of **1** and **2** (4.09 and 3.48 eV, respectively) is similar to the experimentally characterized planar hypercoordinate boron ion with photoelectron spectroscopy (PES), the D_{8h} B_9^- (3.46 (PES), and 3.47 eV (BP86. TZVPP)).[28] The HOMO−LUMO gaps of **1**−**4** (see Table 3) are appreciable and resemble that of the D_{5h} $FeSb_5^{+}$[33] gap (0.85 eV at BP86/TZVPP).[27]

(65) Chen, Z.; Wannere, C. S.; Corminboeuf, C.; Puchta, R.; Schleyer, P. v. R. *Chem. Rev* **2005**, *105*, 3842–3888.
(66) $CMO-NICS(1)_{zz}$ of **2**−**4** could not be computed due to a linear dependency of the basis set.
(67) Pople, J. A. *J. Chem. Phys.* **1956**, *24*, 1111–1112.
(68) Roy, D.; Corminboeuf, C.; Wannere, C.; King, R. B.; Schleyer, P. v. R. *Inorg. Chem.* **2006**, *45*, 8902–8906.
(69) Hoffmann, R.; Schleyer, P. v. R.; Schaefer, H. F., III. *Angew. Chem., Int. Ed.* **2008**, *47*, 7164−7167.

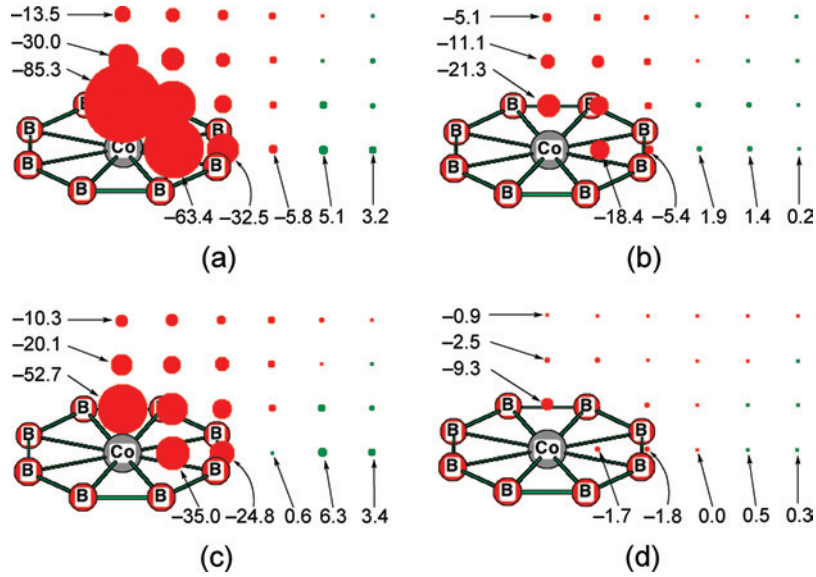

Figure 4. $NICS_{zz}$ grids of (a) $NICS_{zz}$, (b) $NICS_{\pi zz}$, (c) $NICS_{Radzz}$, and (d) $NICS_{dz^2zz}$ of D_{8h} CoB_8^- (**1**) at PW91/TZVPP. Red points indicate diatropic and green points paratropic tensor contributions. NICS values are in ppm.

Table 3. The Lowest Harmonic Vibrational Frequencies (ν_{Min}) and the HOMO−LUMO Gaps of the phTMs **1**−**4**[a]

	ν_{Min} (cm^{-1})	gap (eV)
1	46.7	1.27
2	15.2	0.97
3	38.3	1.03
4	77.8	0.68

[a] Computed at the BP86/TZVPP level.

Additionally, the chemical viability of the phTMs **1**−**4** as isolated singlet, triplet, and quintet species were evaluated by the stochastic search "Kick" method,[60,61] as described above. The potential energy surface scans of **1**−**4** revealed that the singlet planar D_{nh} geometries of **1** and **2** were their global minima. Both anions are excellent candidates for gas phase detection (e.g., by laser ablation/photoelectron spectroscopy). The second-lowest energy isomers of **1** and **2** favor triplet spin states and are 22.3 and 14.9 kcal/mol higher than singlet **1** and **2**, respectively (see Figure 5, **1-aT** and **2-aT**). However, **3** and **4** were not the global minima. The lowest energy isomers of **3** and **4** (Figure 5) were 5.8 and 15.0 kcal/mol more stable than the singlet planar geometries, respectively.

Conclusions

Our theoretical findings suggest that unconventional planar hypercoordinate transition metal compounds, D_{8h} CoB_8^- (**1**) and D_{9h} FeB_9^- (**2**), are global minima and are excellent candidates for gas phase observation. Their unusual planar geometrical preferences and stabilization are due to the strong "double aromatic" interactions between the central TM d AOs and the π/radial MOs of the cyclic boron ligands. The 6 π and 10 radial electrons give rise to strong magnetic diatropicity. The formal electron count shows that the central TMs in **1**−**4** have 18 electrons. However, both **3** and **4** are less stable than nonplanar isomers, triplet **3-aT** and singlet **4-a**, respectively. Nevertheless, even planar transition metal local minima with very high coordination are inherently interesting. We have characterized many other phTM minima; details will subsequently be published.

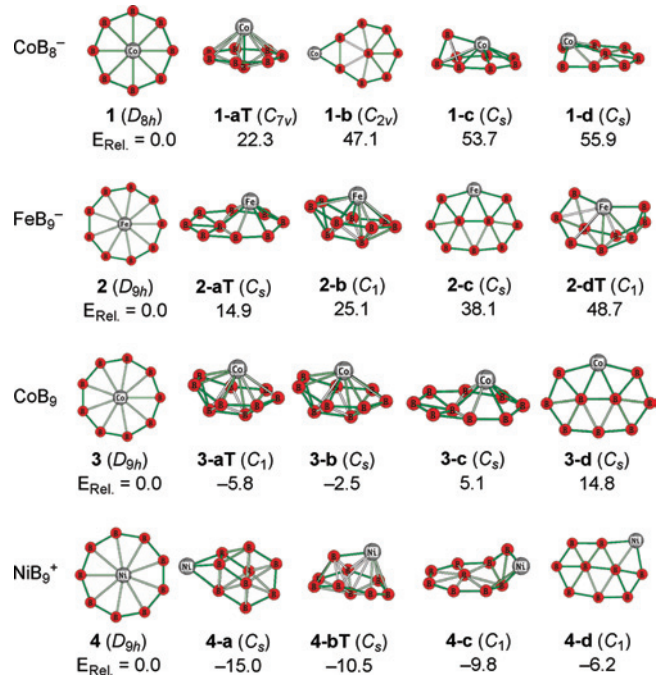

Figure 5. The optimized geometries of the five lowest energy minima of CoB_8^-, FeB_9^-, CoB_9, and NiB_9^+ at BP86/TZVPP. The relative energies (E_{Rel} in kcal/mol) are based on the planar forms. Triplet states are indentified by "T" in the isomer designations.

Acknowledgment. This work was supported by the NSF (CHE-0716718) in the USA and by the 111 Project (B07012) in China. Some computations were performed at the Research Computing Center at the University of Georgia.

Supporting Information Available: Full citation of ref 48, IRC computations of the lowest harmonic vibrational frequency of **1**-**4**, valence MOs of **2**−**4**, and Cartesian coordinates of species **1**−**4**.This material is available free of charge via the Internet at http://pubs.acs.org.

IC800993B